Twist Phase Matching in Two-Dimensional Materials

Hao Hong,[1,2,*,§] Chen Huang,[1,§] Chenjun Ma,[1,§] Jiajie Qi,[1,§] Xuping Shi,[1] Can Liu,[3] Shiwei Wu,[4] Zhipei Sun,[5] Enge Wang,[6,7,8,†] and Kaihui Liu[1,6,7,‡]

[1]*State Key Laboratory for Mesoscopic Physics, Frontiers Science Center for Nano-optoelectronics, School of Physics, Peking University, Beijing, China*

[2]*Interdisciplinary Institute of Light-Element Quantum Materials and Research Centre for Light- Element Advanced Materials, Peking University, Beijing, China*

[3]*Department of Physics, Renmin University of China, Beijing, China*

[4]*State Key Laboratory of Surface Physics and Department of Physics, Fudan University, Shanghai, China*

[5]*Department of Electronics and Nanoengineering and QTF Centre of Excellence, Aalto University, Aalto, Finland*

[6]*International Centre for Quantum Materials, Collaborative Innovation Centre of Quantum Matter, Peking University, Beijing, China*

[7]*Songshan Lake Materials Lab, Institute of Physics, Chinese Academy of Sciences, Dongguan, China*

[8]*School of Physics, Shanghai University, Shanghai, China*

(Received 13 March 2023; accepted 18 October 2023; published 4 December 2023)

Optical phase matching involves establishing a proper phase relationship between the fundamental excitation and generated waves to enable efficient optical parametric processes. It is typically achieved through birefringence or periodic polarization. Here, we report that the interlayer twist angle in two-dimensional (2D) materials creates a nonlinear geometric phase that can compensate for the phase mismatch, and the vertical assembly of the 2D layers with a proper twist sequence generates a nontrivial "twist-phase-matching" (twist-PM) regime. The twist-PM model provides superior flexibility in the design of optical crystals, which can be applied for twisted layers with either periodic or random thickness distributions. The designed crystal from the twisted rhombohedral boron nitride films within a thickness of only 3.2 μm is capable of producing a second-harmonic generation with conversion efficiency of ∼8% and facile polarization controllability that is absent in conventional crystals. Our methodology establishes a platform for the rational design and atomic manufacturing of nonlinear optical crystals based on abundant 2D materials.

DOI: 10.1103/PhysRevLett.131.233801

Nonlinear optical frequency conversion, which arises from the high-order oscillations of electric dipoles within materials driven by a strong optical electric field, plays a crucial role in both classical and quantum optics [1–3]. This nonlinear process is rather weak and requires a long light-matter interaction path to achieve a considerable conversion efficiency. During the propagation of the fundamental excitation light and generated nonlinear signals in thick optical crystals, chromatic dispersion causes a difference in the wave vectors, resulting in destructive interference between parametric waves from different crystal positions and a low conversion efficiency. To compensate for this wave vector difference, the birefringent-phase-matching (birefringent-PM) or quasi-phase-matching (quasi-PM) technique is used to maintain a continuous energy flow from the fundamental to the parametric waves [4–10]. Over the past few decades, numerous materials with high optical nonlinearities have been developed [11] and then fashioned into optical crystals, waveguides, microrings, and microdisks, guided by these two principles [12–15]. These advancements have significantly propelled the development of modern optics and photonics, including quantum light sources, photonic integrated circuits, and ultrafast and high-power lasers.

Two-dimensional (2D) atomically layered materials were demonstrated with ultrahigh nonlinear susceptibilities due to the confined electronic states and reduced electric screening for enhanced light-matter interactions [16–28]. Their strong optical nonlinearities, along with the facile fabrication ability for integration [29], compatibility with Si-based optical chips [30], and rich material library [31], enable 2D materials as promising candidates for functional nonlinear optical crystals. Recently, great efforts have been devoted to fabricating thick 2D material crystals with strong second-harmonic generation (SHG) responses, e.g., MoS_2, $PdSe_2$, $NbOI_2$, and $NbOCl_2$ [32–36]. However, the highest conversion efficiency has just approached 0.2% (Ref. [34]), which is far below that of traditional bulk crystals [11] due to the absence of a suitable phase-matching design. The difficulty lies in the fact that conventional phase-matching techniques are not directly applicable to most kinds of 2D materials. This is because the atomically layered materials suffer from a tendency to cleave along the in-plane direction that constrains cutting

along the other directions in the birefringent-PM design, and their structural domain orientations are difficult to pole by either electric, optical, or magnetic fields for quasi-PM engineering.

As a unique engineering method for 2D materials, the interlayer twist has provided emergent physics and functional applications [37–39]. This twist also produces a new degree of freedom, in principle, for intentionally manipulating the optical phase through stacking 2D layers. In this Letter, we introduce the twist angle into the nonlinear optical crystal design in the example material platform of 2D rhombohedral boron nitride (rBN). We find that the twist angle causes a tunable nonlinear geometric phase, which can be applied to compensate for the phase mismatch in the SHG process.

For a 2D material with in-plane threefold rotation symmetry and mirror symmetry, the nonzero component of the second-order susceptibility is $\chi^{(2)} = \chi_{xxx} = -\chi_{xyy} = -\chi_{yyx} = -\chi_{yxy} = \chi$, where the armchair and zigzag directions lie along the x and y coordinates, respectively. Thus, the second-order polarization can be written as $P_x = \varepsilon_0\chi(E_x^2 - E_y^2)$, $P_y = -2\varepsilon_0\chi E_x E_y$. From the view of the circular polarization, it follows

$$P_- = \sqrt{2}\varepsilon_0\chi E_+^2$$
$$P_+ = \sqrt{2}\varepsilon_0\chi E_-^2, \tag{1}$$

where $\boldsymbol{P} = (P_-, P_+)^T = (P_x - iP_y, P_x + iP_y)^T/\sqrt{2}$, $\boldsymbol{E} = (E_-, E_+)^T = (E_x - iE_y, E_x + iE_y)^T/\sqrt{2})$. Under a rotation operation $R = \left(\begin{smallmatrix} e^{i\theta} & 0 \\ 0 & e^{-i\theta} \end{smallmatrix}\right)$, the polarization evolves as

$$P'_- = \sqrt{2}\varepsilon_0\chi E_+^2 e^{i3\theta}$$
$$P'_+ = \sqrt{2}\varepsilon_0\chi E_-^2 e^{-i3\theta}. \tag{2}$$

Thus, the rotation operation does not change the amplitude of the SHG polarization but instead introduces a $\pm 3\theta$ phase shift. This phase shift is directly derived from the symmetry argument, and is conventionally known as the nonlinear geometric phase (or the nonlinear Pancharatnam-Berry phase in the field of optics [40–44]). It can be appropriately used to compensate for the phase mismatch during the SHG process. More concretely, a simple substitution of Eq. (2) into the nonlinear coupled-wave equations in the slowly varying amplitude approximation of $(\partial \boldsymbol{A}_2/\partial z) = [i2\omega/2\varepsilon_0 cn(2\omega)]\boldsymbol{P_{NL}}(\boldsymbol{K}_2, 2\boldsymbol{\omega})e^{i(2\omega t - k_2 z)}$ leads to twist-angle-dependent nonlinear wave generation as follows:

$$E_{-,2\omega} = \frac{i\sqrt{2}\omega}{cn(2\omega)}\chi E_{+,\omega}^2 \int_0^T e^{i[3\theta(z) - \Delta k z]} dz$$
$$E_{+,2\omega} = \frac{i\sqrt{2}\omega}{cn(2\omega)}\chi E_{-,\omega}^2 \int_0^T e^{i[-3\theta(z) - \Delta k z]} dz, \tag{3}$$

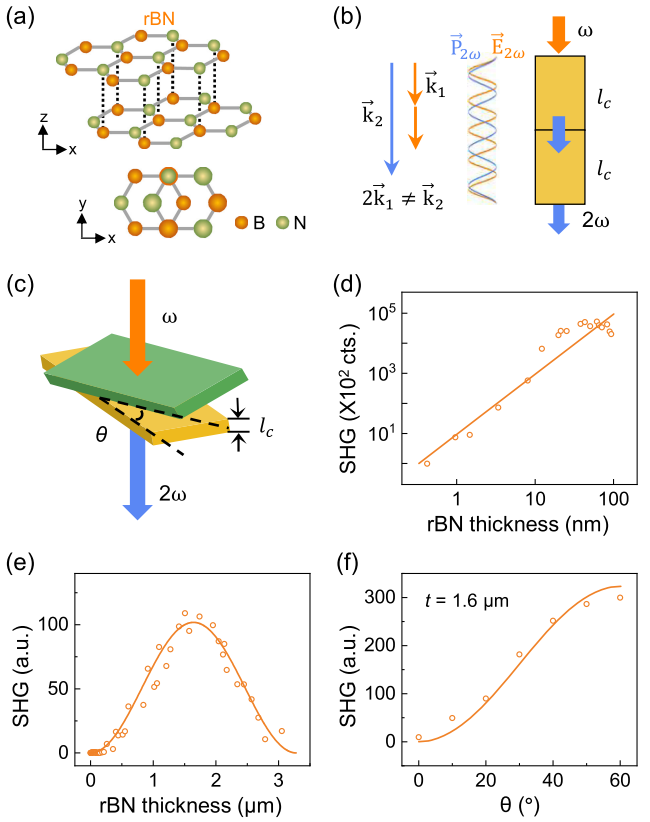

FIG. 1. SHG and phase mismatch in rBN films. (a) Schematics of the atomic structure of rBN. (b) Illustration of the phase mismatch during the propagation of a fundamental excitation wave and the generation of a second harmonic wave in a nonlinear optical crystal. (c) Schematic of a nonlinear optical crystal assembled by two pieces of rBN films with an identical thickness of t and twist angle of θ. (d),(e), Thickness-dependent SHG intensities. A quadratic dependence in (d) evolves to a sinusoidal dependence in (e). (f) Twist angle-dependent SHG output in twisted rBN sketched in (c) with $t = l_c$. The SHG intensity follows a $\sin^2(3\theta/2)$ dependence on θ, as demonstrated by our experiments (hollow circles) and theoretical prediction (solid line).

where $E_{-,2\omega}$, $(E_{+,2\omega})$, and $E_{-,\omega}$, $(E_{+,\omega})$ are the left, (right) circularly polarized components of the second harmonic and fundamental waves, respectively, c is the speed of light in vacuum, $n(2\omega)$ is the refractive index of the second harmonic wave, $\Delta k = k_{2\omega} - 2k_\omega$ and is the wave vector mismatch for SHG, and $\theta(z)$ is the twist angle of the layer at depth z. In Eq. (3), a perfect twist-phase-matching (twist-PM) occurs when $\theta(z) = \Delta k z/3\,(-\Delta k z/3)$, with the incidence of the right (left) circularly polarized fundamental light (circularly polarized fundamental light is essential for the twist-PM design, Supplemental Material [45]).

In our experiments, crystalline rBN films with a parallel-stacking interlayer configuration [Fig. 1(a) and in Supplemental Material [45]] are selected as the engineering platform for the design of nonlinear optical crystals due to their large optical nonlinear susceptibility (see the

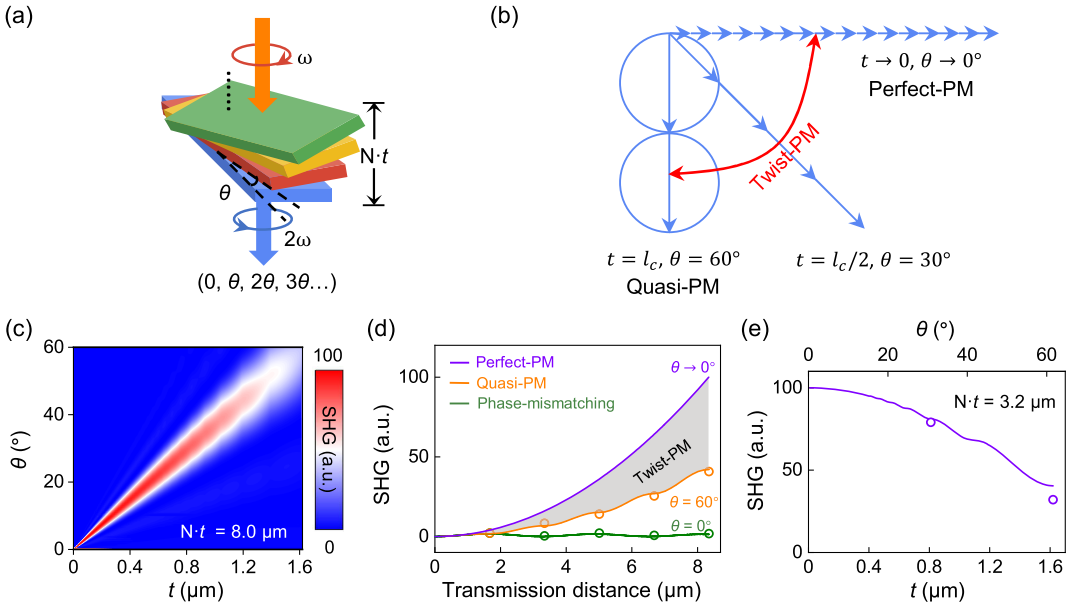

FIG. 2. Twist-PM for efficient SHG in twisted rBN films with identical thickness. (a) Schematic of the attainment of a twist-PM through the assembly of N pieces of rBN films with an identical thickness of t and incremental twist angle sequence. (b) Illustration of the physical picture of the twist-PM process. The electric field of the SHG is indicated as the arc chord vector, whose magnitude is determined by the film's thickness. The twist-PM aligns the arc chord vectors from different rBN films for a strong SHG response. (c) Simulated SHG intensity of the twisted rBN sketched in (a) as a function of t and θ, with a fixed total thickness of 8 μm. (d) Theoretical (solid curves) and experimental (dots) results under different conditions of twisted rBN in (a). The gray area denotes the twist-PM region, with the boundaries of perfect-PM ($\theta \to 0°$, violet curve) and quasi-PM ($\theta = 60°$, origin curve). The green curve represents the phase mismatch ($\theta = 0°$). (e) Output SHG intensity as a function of t and θ under twist-PM conditions. The total thickness is fixed at $2l_c = 3.2$ μm. Twisted crystals under two twist-PM conditions, i.e., $t = l_c(\theta = 60°)$ and $t = l_c/2(\theta = 30°)$, have been measured experimentally (dots) and compared to the theoretical simulations (solid curves).

nonlinear coefficients and band gaps of different materials in Supplemental Material [45]), broadband transparency, excellent physicochemical stability and high laser damage threshold [50–53]. The thickness-dependent SHG intensity under 800 nm fundamental light excitation is measured in a transmission geometry. A quadratic dependence of the output signal on the thickness is expected when the film is thin [Fig. 1(d)] and then evolves to a sinusoidal dependence with increasing thickness [Fig. 1(e)], indicating the appearance of phase mismatch [Fig. 1(b)]. The coherence length (l_c) is determined to be ~1.6 μm.

To apply twist-PM for an efficient SHG process, we assemble two films with thicknesses of l_c and monitor the evolution of the SHG intensity with the twist angle between the two films [Fig. 1(c)]. A $\sin^2(3\theta/2)$ SHG intensity dependence is observed [Fig. 1(f)] due to a phase difference of $(\pi \pm 3\theta)$ between these two films. The output SHG intensity reaches a maximum at an interfilm twist angle of 60°, which corresponds to the conventional quasi-PM condition of periodic antiparallel aligned polarizations (twist angle of 60° equals 180° in rBN crystals).

In fact, the rotational freedom of the twist angles facilitates a new design regime far beyond the conventional quasi-PM. For a simple stacking configuration consisting of N films with an identical thickness of t and twist angle of $\theta_m = (m-1)\theta$ for the m^{th} film [Fig. 2(a)], the output SHG signal is predicted to be as

$$E_{\mp,2\omega} = \frac{i\sqrt{2}\omega}{cn(2\omega)}\chi E_{\pm,\omega}^2 \operatorname{sinc}\left(\frac{\Delta k t}{2}\right) \times \frac{\sin\frac{N}{2}(\pm 3\theta - \Delta k t)}{\sin\frac{1}{2}(\pm 3\theta - \Delta k t)} t \cdot e^{i\frac{N-1}{2}(\pm 3\theta - \Delta k t) - i\frac{\Delta k t}{2}}. \quad (4)$$

The output SHG intensity with different parameters (t, θ) under a fixed total thickness is simulated and shown in Fig. 2(c). The twist-PM can be achieved under the condition of

$$\theta = \pm \Delta k t/3, \quad (5)$$

The physical picture of twist-PM is illustrated in Fig. 2(b). Each layer corresponds to a very small vector that can be viewed as a part of a radius-fixed circle, and each film contributes an arc chord vector, whose magnitude is determined by the film's thickness. The sum of the arc chord vectors corresponds to the electric field of the SHG response. The twist-PM rotates the vectors from different

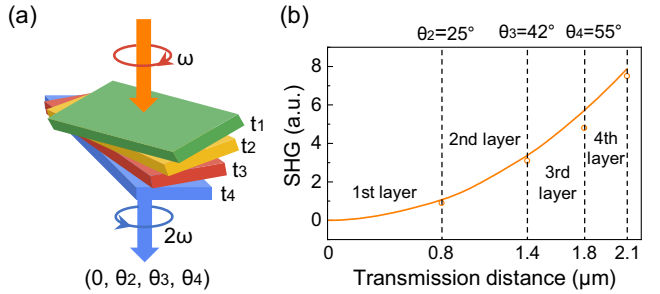

FIG. 3. Twist-PM for efficient SHG in the twisted rBN films with random thicknesses. (a) Schematics of a nonlinear optical crystal assembled by four pieces of the rBN films with different thicknesses of t_1, t_2, t_3, t_4 and a sequence of twist angles. (b) Twist-PM for efficient SHG. For the four rBN films with different thicknesses (800, 600, 400, and 300 nm), the twist-PM can still be fulfilled under twist angles of (0°, 25°, 42°, 55°), as demonstrated theoretically (solid line) and experimentally (hollow circles).

segments in the same direction for a maximum output by a sequence of proper interfilm twist angles.

Evidently, the twist-PM represents a wide phase-matching regime for SHG, and the boundaries of which yield perfect-PM ($\theta \to 0°, t \to 0$) and quasi-PM ($\theta = 60°$, $t = l_c$) [Fig. 2(d)]. Naturally, the stacking of $\theta = 0°$ leads to the phase-mismatching condition. These predictions are highly consistent with our experiments [Fig. 2(d), dots]. The SHG efficiency in the twist-PM regime clearly increases with decreasing t and approaches the maximum at $t \to 0$ [perfect-PM, Fig. 2(e), curve]. Experimentally, we design a total thickness of $2l_c$ under two conditions, i.e., $t = l_c$ (two films, $\theta = 60°$, quasi-PM) and $t = l_c/2$ (four films, $\theta = 30°$, twist-PM). As predicted by our model, the SHG intensity of the twist-PM crystal is approximately two times stronger than that of the quasi-PM crystal [Fig. 2(e), dots]. Since a rBN film of coherence thickness (~1.6 μm) yields a conversion efficiency of 1% (Supplemental Material [45]), the conversion efficiency is expected to be 4% by quasi-PM, but it is promoted to ~8% in the twisted rBN crystal with a total thickness of ~3.2 μm within the twist-PM scenario. This thin crystal is highly desirable for ultrashort pulse as it can potentially minimize the pulse broadening. However, a higher efficiency that is comparable to traditional crystals still needs a thicker stacked rBN crystal.

The twist-PM can also be applied to films with a random thickness distribution [Fig. 3(a)]. The arc chord vectors from different thicknesses of the rBN films can also be aligned with a series of appropriate twist angles. The output SHG electric field can be described as

$$E_{\mp,2\omega} = \frac{i\sqrt{2}\omega}{cn(2\omega)}\chi E_{\pm,\omega}^2 e^{-i\frac{\Delta k t_1}{2}} \times \sum_{m=1}^{N} \exp\left\{ i\left[\pm 3\theta_m - \Delta k\left(\sum_{n=1}^{m} t_n - \frac{1}{2}t_m - \frac{1}{2}t_1 \right) \right] \right\} \times t_m \mathrm{sinc}(\Delta k t_m/2). \quad (6)$$

The twist-PM condition for films with arbitrary thicknesses is as

$$\theta_m = \pm\Delta k\left(\sum_{n=1}^{m} t_n - \frac{1}{2}t_m - \frac{1}{2}t_1 \right)/3, \quad (7)$$

where θ_m and t_m is the twist angle and thickness of the mth film, respectively. This thickness-free choice makes it quite facile and practical to fabricate nonlinear optical crystals from 2D films. Experimentally, we select four films with thicknesses of ~800, 600, 400, and 300 nm. Stacking the film with a sequence of (0°, 25°, 42°, 55°) can ensure that the output SHG would monotonically increase [Fig. 3(b), dots], as predicted by our twist-PM model [Fig. 3(b), curve].

Finally, we demonstrate that twist-PM could not only tune the output intensity but also control the output polarization, an appealing advantage that conventional bulk crystals do not have. From Eq. (3), the mapping from the Stokes parameters of the fundamental wave ($S_{0,\omega}$, $S_{1,\omega}$, $S_{2,\omega}$, $S_{3,\omega}$) to that of the output SHG ($S_{0,2\omega}$, $S_{1,2\omega}$, $S_{2,2\omega}$, $S_{3,2\omega}$) is determined as

$$\begin{aligned}
S_{0,2\omega} &= \frac{2\omega^2}{c^2n^2(2\omega)}\chi^2\left[\left(\frac{S_{0,\omega}+S_{3,\omega}}{2} \right)^2 |B|^2 + \left(\frac{S_{0,\omega}-S_{3,\omega}}{2} \right)^2 |A|^2 \right] \\
S_{1,2\omega} &= 2\mathrm{Re}\left[\frac{2\omega^2}{c^2n^2(2\omega)}\chi^2\left(\frac{S_{1,\omega}+iS_{2,\omega}}{2} \right)^2 AB^* \right] \\
S_{2,2\omega} &= -2\mathrm{Im}\left[\frac{2\omega^2}{c^2n^2(2\omega)}\chi^2\left(\frac{S_{1,\omega}+iS_{2,\omega}}{2} \right)^2 AB^* \right] \\
S_{3,2\omega} &= \frac{2\omega^2}{c^2n^2(2\omega)}\chi^2\left[-\left(\frac{S_{0,\omega}+S_{3,\omega}}{2} \right)^2 |B|^2 + \left(\frac{S_{0,\omega}-S_{3,\omega}}{2} \right)^2 |A|^2 \right],
\end{aligned} \quad (8)$$

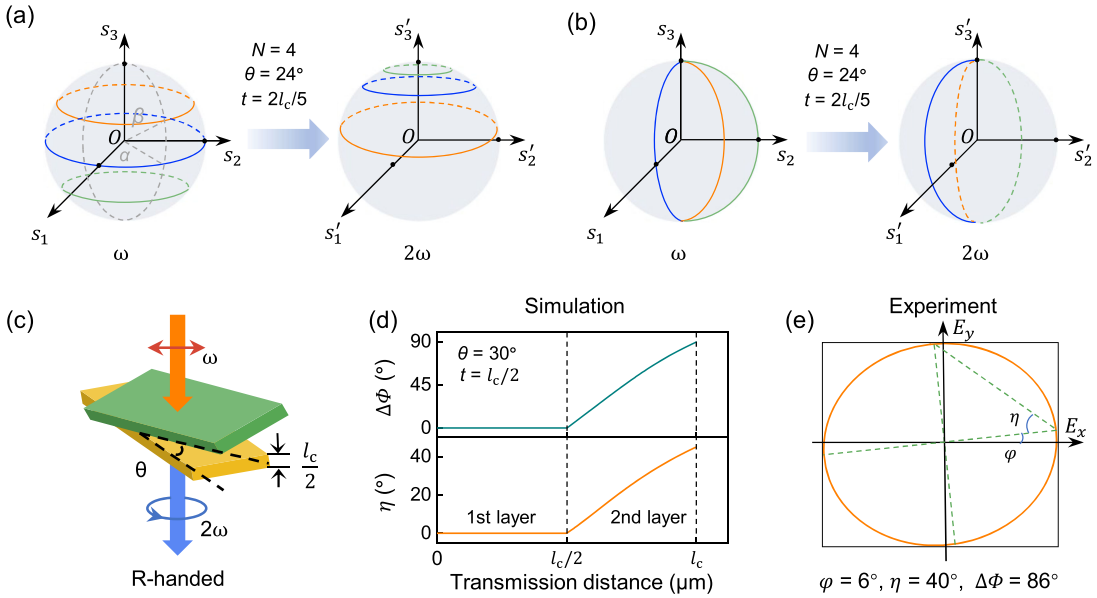

FIG. 4. Polarization control under the twist-PM model. (a),(b), Mappings from the fundamental wave's Poincare sphere to that of the SHG wave. α and β represent the longitude angle and latitude angle of the Poincare sphere, respectively. From our simulation, in a structure consisting of four layers with an identical thickness of $2l_c/5$ and an incremental twist angle of $\theta = 24°$ (follows the twist-PM condition), fundamental waves with $\beta = 60°$, 90°, and 120° will be mapped to the SHG waves with $\beta = 74°$, 28°, and 9.5° on the Poincare sphere (a), and fundamental waves with $\alpha = 0°$, 60°, and 90° will be mapped to the SHG waves with $\alpha = -36°$, $-156°$, and $-216°$ on the Poincare sphere (b). (c) Schematics of a nonlinear optical crystal assembled by the two rBN films with an identical thickness $l_c/2$ and a twist angle $\theta = 30°$. (d),(e), Simulation (d) and experiment (e) of the SHG polarization control in the rBN films sketched in (c). (d) Evolution of the phase difference ($\Delta\Phi$) and ellipticity (η) along with the transmission distance. (e) Polarization measurement of the SHG signal, azimuth angle (φ), phase difference ($\Delta\Phi$) and ellipticity (η) are given. Under linearly polarized light excitation, the SHG output can be tuned to be circularly polarized.

where $A = \int_0^T e^{i[3\theta(z)-\Delta kz]}dz$ and $B = \int_0^T e^{i[-3\theta(z)-\Delta kz]}dz$. This equation demonstrates that the latitude (longitude) lines on the Poincare sphere of the SHG wave are determined solely by the latitude (longitude) lines on the Poincare sphere of the fundamental wave [Figs. 4(a) and 4(b)]. The polarization of the output SHG can be comprehensively and arbitrarily modulated by tuning the polarization of the incident light. A simple prediction is that two pieces of film with $t = l_c/2$ and $\theta = 30°$ would yield a nearly perfect circularly polarized SHG output [Fig. 4(c)], which can be confirmed by our simulation [Fig. 4(d)] and experiment [Fig. 4(e)]. We note that our twist-PM theory can also be applied to design bulk crystals with C_3 symmetry more than 2D materials.

In summary, our Letter presents a twist-PM model that directly introduces a nonlinear geometric phase from twisted 2D layers to compensate for the phase difference in SHG process. It enables a wide regime of phase-matching conditions with high flexibility, versatility and capability for nonlinear optical crystal design (see the comparison between birefringent-PM, quasi-PM and twist-PM in Supplemental Material [45]). This powerful designing ability in twist-PM model, together with rich species, emergent physical properties and facile property tunability in twisted 2D materials, will bring us a new family of nonlinear optical crystals for advanced applications, such as compact parametric amplifiers, on-chip laser sources, and optical modulators.

We acknowledge Professor Yuen-Ron Shen (University of California, Berkeley) for his valuable suggestions and comments on the twist-phase-matching model and rBN crystals. This work is supported by the National Key R&D Program of China (2022YFA1403500 and 2021YFA1400201), National Natural Science Foundation of China (52025023, 51991342, 12374167, 12104018, 12374167 and 12034003), Guangdong Major Project of Basic and Applied Basic Research (2021B0301030002), the Strategic Priority Research Program of Chinese Academy of Sciences (XDB33000000) and the New Cornerstone Science Foundation through the XPLORER PRIZE.

*Corresponding author: haohong@pku.edu.cn
†Corresponding author: egwang@pku.edu.cn
‡Corresponding author: khliu@pku.edu.cn
§These authors contributed equally to this work.

[1] N. Bloembergen, *Nonlinear Optics* (World Scientific, Singapore, 1992).
[2] Y. R. Shen, *The Principles of Nonlinear Optics* (Wiley-VCH, New York, 2003).

[3] R. W. Boyd, *Nonlinear Optics* (Academic Press, New York, 2008).
[4] S. Zhu, Y. Y. Zhu, and N. B. Ming, Science **278**, 843 (1997).
[5] S. N. Zhu, Y. Y. Zhu, Y. Q. Qin, H. F. Wang, C. Z. Ge, and N. B. Ming, Phys. Rev. Lett. **78**, 2752 (1997).
[6] I. Dolev, I. Kaminer, A. Shapira, M. Segev, and A. Arie, Phys. Rev. Lett. **108**, 113903 (2012).
[7] Y. P. Chen, W. R. Dang, Y. L. Zheng, X. F. Chen, and X. W. Deng, Opt. Lett. **38**, 2298 (2013).
[8] B. Q. Chen, C. Zhang, C. Y. Hu, R. J. Liu, and Z. Y. Li, Phys. Rev. Lett. **115**, 083902 (2015).
[9] Z. Cui, D. Liu, J. Miao, A. Yang, and J. Zhu, Phys. Rev. Lett. **118**, 043901 (2017).
[10] J. Lin, N. Yao, Z. Hao, J. Zhang, W. Mao, M. Wang, W. Chu, R. Wu, Z. Fang, L. Qiao, W. Fang, F. Bo, and Y. Cheng, Phys. Rev. Lett. **122**, 173903 (2019).
[11] G. G. Gurzadiân, V. G. Dmitriev, and D. N. Nikogosiân, *Handbook of Nonlinear Optical Crystals* (Springer, New York, 1999).
[12] J. Wang, F. Bo, S. Wan, W. Li, F. Gao, J. Li, G. Zhang, and J. Xu, Opt. Express **23**, 23072 (2015).
[13] J. Lin, Y. Xu, J. Ni, M. Wang, Z. Fang, L. Qiao, W. Fang, and Y. Cheng, Phys. Rev. Appl. **6**, 014002 (2016).
[14] R. Luo, H. Jiang, S. Rogers, H. Liang, Y. He, and Q. Lin, Opt. Express **25**, 24531 (2017).
[15] R. Wolf, Y. Jia, S. Bonaus, C. S. Werner, S. J. Herr, I. Breunig, K. Buse, and H. Zappe, Optica **5**, 872 (2018).
[16] Y. L. Li, Y. Rao, K. F. Mak, Y. M. You, S. Y. Wang, C. R. Dean, and T. F. Heinz, Nano Lett. **13**, 3329 (2013).
[17] C. J. Kim, L. Brown, M. W. Graham, R. Hovden, R. W. Havener, P. L. McEuen, D. A. Muller, and J. Park, Nano Lett. **13**, 5660 (2013).
[18] J.-L. Cheng, N. Vermeulen, and J. Sipe, New J. Phys. **16**, 053014 (2014).
[19] K. L. Seyler, J. R. Schaibley, P. Gong, P. Rivera, A. M. Jones, S. F. Wu, J. Q. Yan, D. G. Mandrus, W. Yao, and X. D. Xu, Nat. Nanotechnol. **10**, 407 (2015).
[20] H. Z. Liu, Y. L. Li, Y. S. You, S. Ghimire, T. F. Heinz, and D. A. Reis, Nat. Phys. **13**, 262 (2017).
[21] N. Yoshikawa, T. Tamaya, and K. Tanaka, Science **356**, 736 (2017).
[22] J. D. Cox, A. Marini, and F. J. G. de Abajo, Nat. Commun. **8**, 14380 (2017).
[23] T. Jiang, D. Huang, J. L. Cheng, X. D. Fan, Z. H. Zhang, Y. W. Shan, Y. F. Yi, Y. Y. Dai, L. Shi, K. H. Liu, C. G. Zeng, J. Zi, J. E. Sipe, Y. R. Shen, W. T. Liu, and S. W. Wu, Nat. Photonics **12**, 634 (2018).
[24] G. Soavi, G. Wang, H. Rostami, D. G. Purdie, D. De Fazio, T. Ma, B. R. Luo, J. J. Wang, A. K. Ott, D. Yoon, S. A. Bourelle, J. E. Muench, I. Goykhman, S. Dal Conte, M. Celebrano, A. Tomadin, M. Polini, G. Cerullo, and A. C. Ferrari, Nat. Nanotechnol. **13**, 583 (2018).
[25] J. D. Caldwell, I. Aharonovich, G. Cassabois, J. H. Edgar, B. Gil, and D. N. Basov, Nat. Rev. Mater. **4**, 552 (2019).
[26] K. Y. Yao *et al.*, Sci. Adv. **7**, eabe8691 (2021).
[27] H. Hong *et al.*, Nat. Photonics **15**, 510 (2021).
[28] K. Khaliji, L. Martín-Moreno, P. Avouris, S.-H. Oh, and T. Low, Phys. Rev. Lett. **128**, 193902 (2022).
[29] F. Liu, W. J. Wu, Y. S. Bai, S. H. Chae, Q. Y. Li, J. Wang, J. Hone, and X. Y. Zhu, Science **367**, 903 (2020).
[30] D. Akinwande, C. Huyghebaert, C. H. Wang, M. I. Serna, S. Goossens, L. J. Li, H. S. P. Wong, and F. H. L. Koppens, Nature (London) **573**, 507 (2019).
[31] N. Mounet, M. Gibertini, P. Schwaller, D. Campi, A. Merkys, A. Marrazzo, T. Sohier, I. E. Castelli, A. Cepellotti, G. Pizzi, and N. Marzari, Nat. Nanotechnol. **13**, 246 (2018).
[32] M. Zhao, Z. L. Ye, R. Suzuki, Y. Ye, H. Y. Zhu, J. Xiao, Y. Wang, Y. Iwasa, and X. Zhang, Light Sci. Appl. **5**, e16131 (2016).
[33] J. Yu, X. F. Kuang, J. Z. Li, J. H. Zhong, C. Zeng, L. K. Cao, Z. W. Liu, Z. X. S. Zeng, Z. Y. Luo, T. C. He, A. L. Pan, and Y. P. Liu, Nat. Commun. **12**, 1083 (2021).
[34] I. Abdelwahab, B. Tilmann, Y. Z. Wu, D. Giovanni, I. Verzhbitskiy, M. L. Zhu, R. Berte, F. Y. Xuan, L. D. Menezes, G. Eda, T. C. Sum, S. Y. Quek, S. A. Maier, and K. P. Loh, Nat. Photonics **16**, 644 (2022).
[35] X. Y. Xu, C. Trovatello, F. Mooshammer, Y. M. Shao, S. Zhang, K. Y. Yao, D. N. Basov, G. Cerullo, and P. J. Schuck, Nat. Photonics **16**, 698 (2022).
[36] Q. Guo *et al.*, Nature (London) **613**, 53 (2023).
[37] N. P. Wilson, W. Yao, J. Shan, and X. Xu, Nature (London) **599**, 383 (2021).
[38] K. F. Mak and J. Shan, Nat. Nanotechnol. **17**, 686 (2022).
[39] D. Huang, J. Choi, C.-K. Shih, and X. Li, Nat. Nanotechnol. **17**, 227 (2022).
[40] S. Pancharatnam, Proc. Ind. Acad. Sci. **44**, 247 (1956).
[41] M. V. Berry, J. Mod. Opt. **34**, 1401 (1987).
[42] Z. e. Bomzon, G. Biener, V. Kleiner, and E. Hasman, Opt. Lett. **27**, 1141 (2002).
[43] M. Tymchenko, J. S. Gomez-Diaz, J. Lee, N. Nookala, M. A. Belkin, and A. Alù, Phys. Rev. Lett. **115**, 207403 (2015).
[44] G. Li, S. Chen, N. Pholchai, B. Reineke, P. W. H. Wong, E. Y. B. Pun, K. W. Cheah, T. Zentgraf, and S. Zhang, Nat. Mater. **14**, 607 (2015).
[45] See Supplemental Material at http://link.aps.org/supplemental/10.1103/PhysRevLett.131.233801 for additional experiment details, which includes Refs. [46–49].
[46] K. R. Allakhverdiev, M. Ö. Yetis, S. Özbek, T. K. Baykara, and E. Yu. Salaev, Laser Phys. **19**, 1092 (2009).
[47] D. J. Clark, V. Senthilkumar, C. T. Le, D. L. Weerawarne, B. Shim, J. I. Jang, J. H. Shim, J. Cho, Y. Sim, M.-J. Seong, S. H. Rhim, A. J. Freeman, K.-H. Chung, and Y. S. Kim, Phys. Rev. B **90**, 121409(R) (2014).
[48] L. Hu, X. Huang, and D. Wei, Phys. Chem. Chem. Phys. **19**, 11131 (2017).
[49] H. G. Rosa, Y. W. Ho, I. Verzhbitskiy, M. J. F. L. Rodrigues, T. Taniguchi, K. Watanabe, G. Eda, V. M. Pereira, and J. C. V. Gomes, Sci. Rep. **8**, 10035 (2018).
[50] Y. Kubota, K. Watanabe, O. Tsuda, and T. Taniguchi, Science **317**, 932 (2007).
[51] G. Cassabois, P. Valvin, and B. Gil, Nat. Photonics **10**, 262 (2016).
[52] N. Tancogne-Dejean and A. Rubio, Sci. Adv. **4**, eaao5207 (2018).
[53] A. Autere, H. Jussila, Y. Y. Dai, Y. D. Wang, H. Lipsanen, and Z. P. Sun, Adv. Mater. **30**, 1705963 (2018).